Control of Grid Connected Photovoltaic Systems with Microinverters

New Theoretical Design and Numerical Evaluation

Yahya, Abdelhafid; El Fadil, Hassan; Oulcaid, Mustapha; Ammeh, Leila; Giri, Fouad; Guerrero, Josep M.

Published in:
Asian Journal of Control

DOI (link to publication from Publisher):
10.1002/asjc.1704

Publication date:
2018

Document Version
Early version, also known as pre-print

Control of Grid Connected Photovoltaic Systems With Microinverters – New Theoretical Design and Numerical Evaluation

Abdelhafid Yahya[1], Hassan El Fadil [2*], Mustapha Oulcaid[3], Leila Ammeh[4], Fouad Giri [5], Josep M. Guerrero [6]

[1-4] LGS Laboratory, ENSA, Ibn Tofail University, 14000, Kénitra, Morocco.
(e-mails: yaabha2@gmail.com, elfadilhassan@yahoo.fr, oulcaid02@gmail.com, ammeh.leila@gmail.com,)
[5] LAC Laboratory, Caen University, Bd Marechal Juin, B.P 8156, 14032, Caen, France
(e-mail: fouad.giri@unicaen.fr)
[6] Department of Energy Technology, Aalborg University, 9220 Aalborg East, Denmark,
(e-mail: joz@et.aau.dk)
[*]Corresponding author

Abstract. The problem of controlling grid connected photovoltaic (PV) systems, that are driven with microinverters, is addressed. The systems to be controlled consist of a solar panel, a boost dc-dc converter, a DC link capacitor, a single-phase full-bridge inverter, a filter inductor and an isolation transformer. We seek controllers that are able to simultaneously achieve four control objectives, namely: (i) asymptotic stability of the closed loop control system; (ii) maximum power point tracking (MPPT) of the PV module; (iii) tight regulation of the DC bus voltage; (iv) and unity power factor (PF) in the grid. To achieve these objectives, a new multiloop nonlinear controller is designed using the backstepping design technique. A key feature of the control design is that it relies on an averaged nonlinear system model accounting, on the one hand, for the nonlinear dynamics of the underlying boost converter and inverter and, on the other, for the nonlinear characteristic of the PV panel. To achieve the MPPT objective, a power optimizer is designed that computes online the optimal PV panel voltage used as reference signal by the PV voltage regulator. It is formally shown that the proposed controller meets all the objectives. This theoretical result is confirmed by numerical simulation tests.

Keywords: microinverter; photovoltaic; nonlinear control; MPPT; PFC.

1. Introduction

In the recent years, considerable increase in energetic demand, together with the requirement of gas emission reduction, have caused a deep metamorphose of the electricity market worldwide. Major manifestations of this evolution are market deregulation and energy source diversification. In this respect, renewable energy resources, especially wind turbines, photovoltaic panels, gas turbines and fuel cells, have gained a significant interest. In particular, solar energy is considered as one of the most useful natural energy sources because it is free, abundant, pollution-free, and most widely distributed. It can be used either as standalone apparatus (in isolated regions) or as grid interactive power source (in urban areas), [1]. On the other hand, the significant progress made over the few past years in solar cells technology, improving their efficiency and reliability, has triggered a rapid growth of solar industry, contributing to the popularisation of PV systems especially in distributed generation (DG) at medium and

low voltages power systems. Implementing distributed energy resources (DER), into interconnected grids could be part of the solution to meet the rising electricity demand [2-5]. DG technologies are currently being improved through several research projects toward the development of smart grids.

PV energy applications are divided into two categories: stand-alone systems and grid-connected systems. Stand-alone systems require a battery bank to store the PV energy; this is suitable for low-power systems. On the other hand, grid-connected PV systems do not require battery banks; they are resorted generally in high power applications. The main purpose of the grid-connected system is to extract the maximal possible quantity of solar array energy and restitute it to grid with a unity power factor, despite changing atmospheric conditions (temperature and radiation).

PV grid-connected systems represent the most important field applications of solar energy [6-11]. In general, a photovoltaic grid-connected system can be seen as a two-stage grid-connected inverter (Fig.1). The first stage is a dc-dc converter controlled so that the photovoltaic system operates in optimal condition i.e. seeking maximum power point tracking (MPPT). The second stage is a dc-ac converter that controlled in a way that allows a grid connection with a unity power factor (PF). To this end, the output current (entering the grid) must be sinusoidal and in phase with the grid voltage. The dc-dc and dc-ac converters operate independently making easier the whole system control.

This study is focusing on the problem of controlling photovoltaic grid connected systems with single-phase microinverters (Fig. 1). A suitable control strategy is one that is able to simultaneously ensure the four objectives: (i) asymptotic stability of the closed loop control system; (ii) MPPT of the PV module; (iii) tight regulation of the DC bus voltage; (iv) and unity PF in the grid. These objectives must be achieved despite changes of the climatic variables (temperature and radiation). The main contribution of the paper is the development of a new theoretical framework for accurately stating and dealing with the above control problem. This theoretical framework includes the accurate modelling of photovoltaic grid connected systems with single-phase microinverter, the design of a multiloop nonlinear controller on the basis of a large-signal nonlinear model of the controlled system, the formal analysis of the resulting closed-loop control system. The main features of the proposed control design and analysis are threefold:

1) A new power optimizer designed to achieve the MPPT purpose is proposed. Specifically, the power optimizer is expected to compute on-line the optimal voltage value V_m so that, if the PV voltage v_p is made equal to V_m then, maximal power is extracted from the PV panel, and then transmitted to the grid through the inverter. Presently, the power optimizer design is based on the power-voltage (P-V) characteristic. This characteristic is highly nonlinear and its shape depends on the radiation and the temperature. These difficulties make the MPPT task a highly complex problem. Most existing works have proposed heuristic search algorithms, e.g. perturb-and-observe

[12,13], incremental conductance [14,15], fuzzy logic [16,17], etc. The drawback of these solutions is a slow convergence rate and reduced accuracy. Our solution enjoys a rapid accurate convergence to the MPP. This achievement is made possible because our approach involves a reference voltage optimization technique designed using a rigorous modelling of the dependence of the optimal couples (V_m, P_m) on radiation and temperature. One key idea in the power optimizer design is to notice that the optimal reference voltage is related to the PV power by a well defined nonlinear function, the parameters of which are affine functions of the temperature.

2) One more feature of the proposed MPPT solution is that no radiation sensor is required. This sensorless feature constitutes a major achievement because the prices of solar radiation sensors are generally high. Moreover, less sensors in the proposed solution improves its reliability and so reduces its exploitation cost.

3) Owing to control design, our solution involves three regulators designed on the basis of the nonlinear system model. Furthermore, the control design takes benefits of advanced nonlinear control design techniques e.g. the backstepping technique. Moreover, the control design is backed with a rigorous formal performance analysis, involving tools from Lyapunov stability theory, showing that all control objectives are actually achieved. In this respect, our work contrasts with most previous works [18-23]. In the latter, the control design has generally been performed based on approximate linear models while formal performance analysis has generally been missing

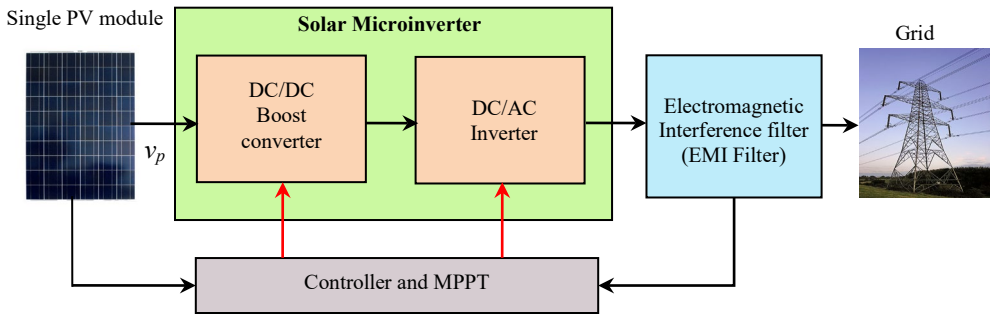

Fig.1: Solar Microinverter Block Diagram

The paper is organized as follows: the single phase grid connected PV system is described and modelled in Section 2. Section 3 is devoted to controller design and analysis. The controller tracking performances are illustrated by numerical simulation in Section 4. A conclusion and reference list end the paper.

2. Presentation and Modelling of Grid Connected PV System

A typical configuration of single-phase microinverter for photovoltaic grid connected applications is shown in Fig.2. It consists of the following parts:

- a solar panel, an input capacitor C_i,

- a boost dc-dc converter (used for boosting the array voltage and achieving MPPT for PV array),

- a DC link capacitor C_{dc}, a single-phase full-bridge inverter including four power semiconductors (resorted to ensure unity PF DC-AC power conversion),

- a filter inductor L_g, and an isolation transformer.

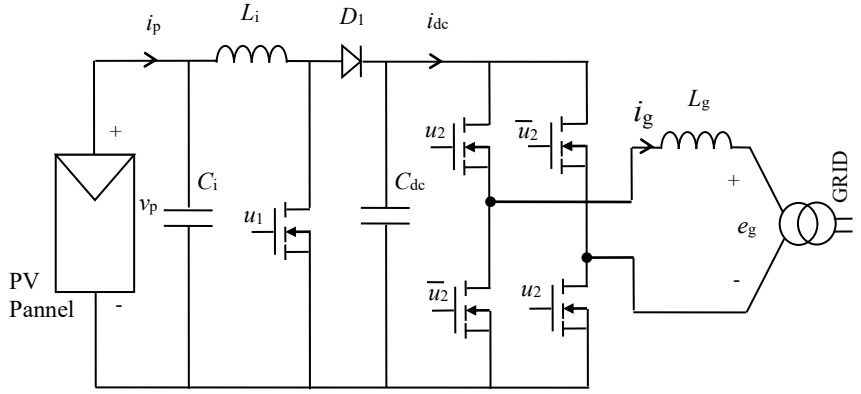

Fig.2: Single phase grid connected PV system

2.1. PV array model

Typical (I_p-V_p) characteristics of solar cells arranged in N_p-parallel and N_s-series can be found in many places (see e.g. [24-27]. The PV array module considered in this paper is of type NU-183E1. The corresponding electrical characteristics are listed in Table 1.

Table 1. Electrical specifications for the solar module NU-183E1

Parameter	Symbol	Value
Maximum Power	P_m	183.1W
Short circuit current	I_{scr}	8.48 A
Open circuit voltage	V_{oc}	30.1V
Maximum power voltage	V_m	23.9 V
Maximum power current	I_m	7.66A
Number of parallel cells	N_p	1
Number of series cells	N_s	48

2.2. Boost Converter Modeling

The control input u_1 of the boost converter is a PWM signal taking values in the set $\{0,1\}$. Applying Kirchoff's laws, successively with $u_1 = 1$ and $u_1 = 0$, to the boost converter circuit of Fig. 2 one obtains the following instantaneous model:

$$\frac{dv_p}{dt} = \frac{1}{C_i}(i_p - i_{Li}) \tag{1a}$$

$$\frac{di_{Li}}{dt} = -(1-u_1)\frac{v_{dc}}{L_i} - \frac{R_i}{L_i}i_{Li} + \frac{v_p}{L_i} \tag{1b}$$

$$\frac{dv_{dc}}{dt} = (1-u_1)\frac{i_{Li}}{C_{dc}} - \frac{1}{C_{dc}}i_{dc} \tag{1c}$$

where R_i is the equivalent series resistance (ESR) of input inductance L_i.

2.3. Single-Phase Full-Bridge Inverter Modeling

The control input u_2 of the single-phase full-bridge inverter is also a PWM signal taking values in the set $\{0,1\}$. Applying Kirchoff's laws, successively with $u_2 = 1$ and $u_2 = 0$, to the inverter circuit of Fig. 2 one obtains the following instantaneous model:

$$\frac{di_{Lg}}{dt} = (2u_2 - 1)\frac{v_{dc}}{L_g} - \frac{R_g}{L_g}i_{Lg} - \frac{e_g}{L_g} \tag{2a}$$

$$i_{dc} = (2u_2 - 1)i_{Lg} \tag{2b}$$

where R_g is the ESR of the filter inductance L_g.

2.4. Overall system model

The instantaneous model (1a-c, 2a-b) of the single-phase grid connected photovoltaic system is useful for simulator design. But, it is not suitable for controller design because it involves binary control inputs u_1 and u_2. For control design purpose, it is more convenient to consider the following averaged model [28]:

$$\frac{dx_1}{dt} = \frac{1}{C_i}(\bar{i}_p - x_2) \tag{3a}$$

$$\frac{dx_2}{dt} = -(1-\mu_1)\frac{x_3}{L_i} - \frac{R_i}{L_i}x_2 + \frac{x_1}{L_i} \tag{3b}$$

$$\frac{dx_3}{dt} = (1-\mu_1)\frac{x_2}{C_{dc}} - (2\mu_2 - 1)\frac{x_4}{C_{dc}} \tag{3c}$$

$$\frac{dx_4}{dt} = (2\mu_2 - 1)\frac{x_3}{L_g} - \frac{R_g}{L_g}x_4 - \frac{e_g}{L_g} \tag{3d}$$

where x_1, x_2, x_3, x_4, $\bar{i}_p$, μ_1 and μ_2 denote the average values, respectively of v_p, i_{Li}, v_{dc}, i_{Lg}, i_p, u_1 and u_2. Averaging of all variables is performed over switching periods. Consequently, the quantities μ_1 and μ_2, commonly called duty ratios, vary continuously in the interval $[0,1]$ and act as the input control signals.

3. Controller Design

In this section, we aim at designing a controller that will be able to ensure, in addition to closed loop system global stability, perfect MPPT (whatever the position of the PV panel). Specifically, the controller must enforce the voltage x_1 to track, as accurately as possible, the unknown (and slowly varying) voltage V_m. Note that V_m is unknown because it depends on the temperature T and the solar radiation λ, which is not supposed to be accessible to measurements. Additional control objectives include unity PF connection to the grid and tight regulation of the dc bus voltage x_3.

3.1. Controlling the boost converter to meet MPPT

Recall that the control objective is to enforce the voltage x_1 to track the optimal point V_m. To this end, the backstepping design technique is used [29-31]. Then, the control design applies in a systematic way, in two steps.

Design Step 1. Let us introduce the following tracking error:

$$z_1 = x_1 - V_m \tag{4}$$

The definition of the optimal voltage V_m will be investigated later in this paper.

Achieving the MPPT objective amounts to enforcing the error z_1 to vanish. To this end, the dynamics of z_1 have to be clearly defined. Deriving (4), it follows from (3a) that

$$\dot{z}_1 = \frac{1}{C_i}(\bar{i}_p - x_2) - \dot{V}_m \tag{5}$$

In the above equation, the quantity x_2 / C_i stands as a virtual control variable. To determine the trajectory of this virtual control variable, the following Lyapunov function is considered:

$$V_1 = 0.5 z_1^2 \tag{6}$$

The time-derivative of V_1 along the trajectory of (5) is given by:

$$\dot{V}_1 = z_1 \left(\frac{-x_2}{C_i} + \frac{\bar{i}_p}{C_i} - \dot{V}_m \right) \tag{7}$$

Equation (7) shows that the tracking error z_1 can be regulated to zero if $x_2 / C_i = \alpha_1$ where α_1 is a stabilizing function defined by

$$\alpha_1 = \frac{i_p}{C_i} + c_1 z_1 - \dot{V}_m \tag{8}$$

where $c_1 > 0$ being a design parameter. Since x_2 / C_i is not the actual control input, one can only seek the convergence of the error $x_2 / C_i - \alpha_1$ to zero. We then define the following second error variable:

$$z_2 = x_2 / C_i - \alpha_1 \tag{9}$$

The next step is to determine a variation law for control signal μ_1 so that the set of errors z_1 and z_2 vanish asymptotically. But, let us first establish some useful equations. Equation (5) becomes, using (9):

$$\dot{z}_1 = -c_1 z_1 - z_2 \tag{10}$$

Also, the derivative (7) of the Lyapunov function is rewritten as:

$$\dot{V}_1 = -c_1 z_1^2 - z_1 z_2 \tag{11}$$

Design Step 2. The objective now is to enforce the error variables (z_1, z_2) to vanish. To this end, let us first determine the dynamics of z_2. Deriving (9) and using (3b), and (10), one obtains

$$\dot{z}_2 = -(1-\mu_1)\frac{x_3}{L_i C_i} - \frac{R_i}{L_i C_i} x_2 + \frac{x_1}{L_i C_i} - \frac{1}{C_i}\frac{d\bar{i}_p}{dt} + c_1^2 z_1 + c_1 z_2 + \ddot{V}_m \tag{12}$$

We are finally in a position to make a convenient choice of the control signal μ_1 to stabilize the whole system with state vector (z_1, z_2). To this end, consider the augmented Lyapunov function candidate:

$$V_2 = V_1 + 0.5 z_2^2 = 0.5 z_1^2 + 0.5 z_2^2 \tag{13}$$

Using (10), one gets the time-derivative:

$$\dot{V}_2 = \dot{V}_1 + z_2 \dot{z}_2 = -c_1 z_1^2 - c_2 z_2^2 + z_2\left[-z_1 + c_2 z_2 + \dot{z}_2\right] \tag{14}$$

with $c_2 > 0$ a design parameter. Equation (14) shows that the equilibrium (z_1, z_2)=(0,0) is globally asymptotically stable if one sets:

$$\dot{z}_2 = -c_2 z_2 + z_1 \tag{15}$$

Combining (12) and (15), one gets the following control law:

$$\mu_1 = 1 - \frac{1}{x_3}\left\{L_i C_i\left[(c_1^2 - 1) z_1 + (c_1 + c_2) z_2 + \ddot{V}_m\right] + x_1 - R_i x_2 - L_i \dot{\bar{i}}_p\right\} \tag{16}$$

3.2. Controlling the inverter to meet unity PF in the grid and regulation of the dc bus voltage objectives

3.2.1. Unity PF objective

The objective of unity PF means that the grid current i_{Lg} should be sinusoidal and in phase with the AC grid voltage e_g. We therefore seek a regulator that enforces the current x_4 to track the reference signal x_4^* of the form:

$$x_4^* = \beta e_g \tag{17}$$

with β is any real positive parameter (although transient time-variation are allowed). The regulator will

now be designed using again the backstepping technique. Let us introduce the following current tracking error:

$$z_3 = x_4 - x_4^* \tag{18}$$

In view of (3d), the dynamics of the above error are described by the following equation:

$$\dot{z}_3 = \dot{x}_4 - \dot{x}_4^* = (2\mu_2 - 1)\frac{x_3}{L_g} - \frac{R_g}{L_g}x_4 - \frac{e_g}{L_g} - \dot{x}_4^* \tag{19}$$

To get a stabilizing control law for this first-order system, consider the following quadratic Lyapunov function:

$$V_3 = 0.5 z_3^2 \tag{20}$$

It can be easily checked that the time-derivative $\dot{V}_3$ is a negative definite function of z_3 if the control input μ_2 is chosen to be:

$$\mu_2 = \frac{1}{2} + \frac{1}{2x_3}\left\{R_g x_4 + e_g + L_g\left(-c_3 z_3 + \dot{x}_4^*\right)\right\} \tag{21}$$

where $c_3 > 0$ is a design parameter. Indeed, with this choice one has:

$$\dot{z}_3 = -c_3 z_3 \tag{22}$$

$$\dot{V}_3 = -c_3 z_3^2 \tag{23}$$

These equations show that the equilibrium $(z_3 = 0)$ of (19) is globally asymptotically stable. Consequently, the unit PF objective is asymptotically achieved.

3.2.2. DC bus voltage regulation objective

Now, the aim is to design a variation law for the ratio β in (17) so that the inverter dc input voltage $x_3 =< v_{dc} >$ is steered to a given constant reference $V_d > 0$. To this end, the following PI control law is used:

$$\beta = G_{pi}(s)\varepsilon_{dc} \tag{24a}$$

with:

$$G_{pi}(s) = k_i \frac{(1 + \tau_i s)}{\tau_i s} \tag{24b}$$

$$\varepsilon_{dc} = x_3 - V_d \tag{24c}$$

The performances of the controller, consisting of the control laws (24a-c), (21) and (16) will be described later in Theorem1.

3.3. Voltage-reference optimizer for MPPT

The optimizer we are seeking is expected to compute on-line the optimal voltage V_m so that, if the voltage v_p is made equal to V_m then, maximal power is extracted from the PV panel, and then transmitted to the grid through the inverter. A major feature of the proposed optimizer is that it does not require any radiation sensor (the prices of such sensors are much higher than those of temperature). Presently, the design of the voltage-reference optimizer is performed on the basis of the power-voltage (P-V) characteristic. The summits of these curves correspond to the maximum extractable power P_m and so represent the optimal points. Each one of these points is characterized by the optimal voltage V_m. A set of optimal couples (V_m, P_m), for different radiations and temperatures, is thus collected and plotted in Fig. 3. Then, all couples corresponding to each fixed temperature are interpolated to get the following function:

$$V_m = a\exp\left(-b\sqrt{P_m}\right)+c \tag{25}$$

Of course, the coefficients a, b and c depend on the considered fixed temperature (see Table 2).

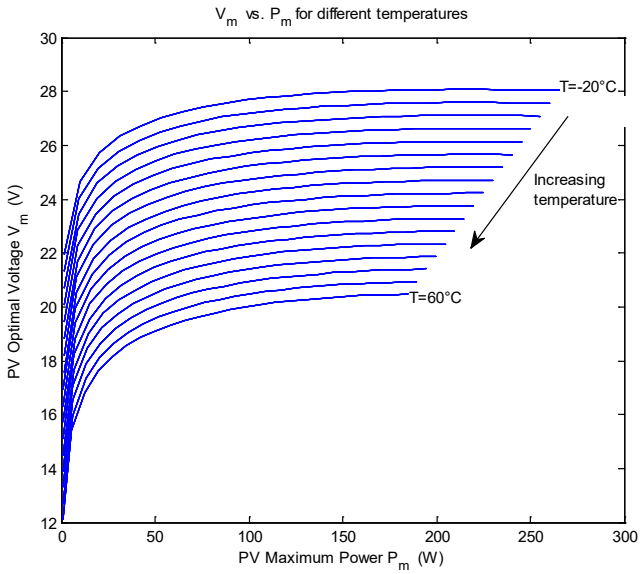

Fig.3: P–V Optimal power-voltage characteristic obtained from the interpolation of points (V_m, P_m) for NU-183E1 module

Table 2. Values of coefficients *a*, *b* and *c* involved in (25) for different temperatures

Temperature T (°C)	*a*	*b*	*c*
-20	-9.007	0.2850	28.21
-15	-9.145	0.2839	27.73
-10	-9.278	0.2824	27.25
-5	-9.414	0.2813	26.77
0	-9.549	0.2804	26.30

5	-9.694	0.2804	25.82
10	-9.817	0.2796	25.35
15	-9.941	0.2796	24.87
20	-10.06	0.2792	24.40
25	-10.19	0.2795	23.93
30	-10.30	0.2797	23.46
35	-10.41	0.2798	22.99
40	-10.52	0.2806	22.52
45	-10.62	0.2808	22.06
50	-10.72	0.2818	21.59
55	-10.81	0.2822	21.13
60	-10.90	0.2835	20.67

Remarks 1.1) By direct inspection of Table 3, one sees that the parameters *a* and *c* are highly dependent on temperature while the parameter *b* is approximately constant $b \approx 0.28$.

2) Interestingly, Fig. 4 shows that the parameters *a* and *c* are linearly dependent on temperature *T*.

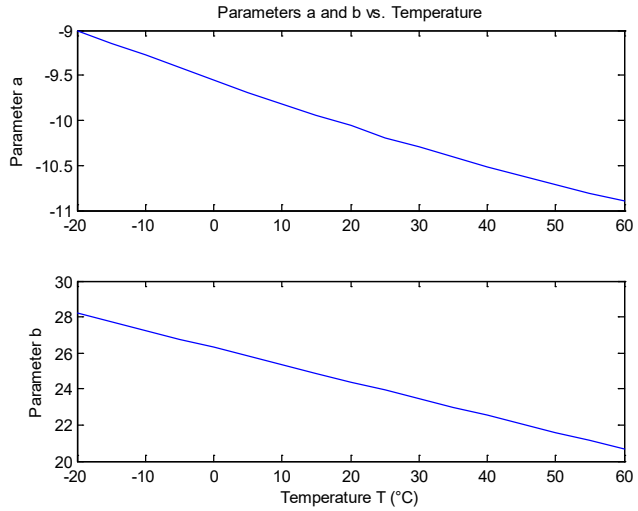

Fig.4: Variation of the parameters *a* and *b* with temperature.

Using the previous observations, it follows from (25) that the optimal voltage V_m is generated as follows:

$$V_m = (-23\times10^{-3}T - 9.55)\exp\left(-0.28\sqrt{P_m}\right) + (-94.2\times10^{-3}T + 26.3) \tag{26}$$

This expression defines the PV power optimizer, generating online the optimal voltage V_m from the measured variables (PV voltage, PV current and Temperature). This optimizer is also represented by the block diagram of Fig. 5.

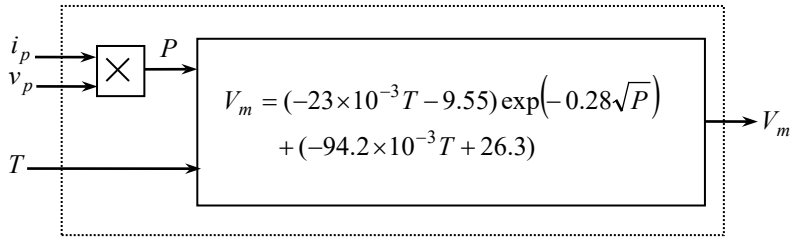

Fig.5: PV power optimizer, calculating on-line the optimal voltage V_m

Let us illustrate the MPPT operation considering the situation of Fig. 6. It is considered there that the PV panel, operating under a given radiation λ_0 and temperature T_0, is initially at some operation point $M_0(V_{m0}, P_{m0})$. For this temperature T_0, the optimal power-voltage characteristic is also plotted (dashed red curve) according to Fig.3. Then, the optimizer generates a new optimal voltage V_{m1} driving the system to the operation point $M_1(V_{m1}, P_{m0})$. This new voltage V_{m1} entails the generation of a new power P_{m1}. Then, the operation point immediately gets shifted to $M_2(V_{m1}, P_{m1})$. Then, the optimizer enforces the system to operate with the new optimal voltage V_{m2} (operation point $M_3(V_{m2}, P_{m1})$). This procedure is continuously repeated until the top point M_5 is reached which clearly corresponds to the desired MPP.

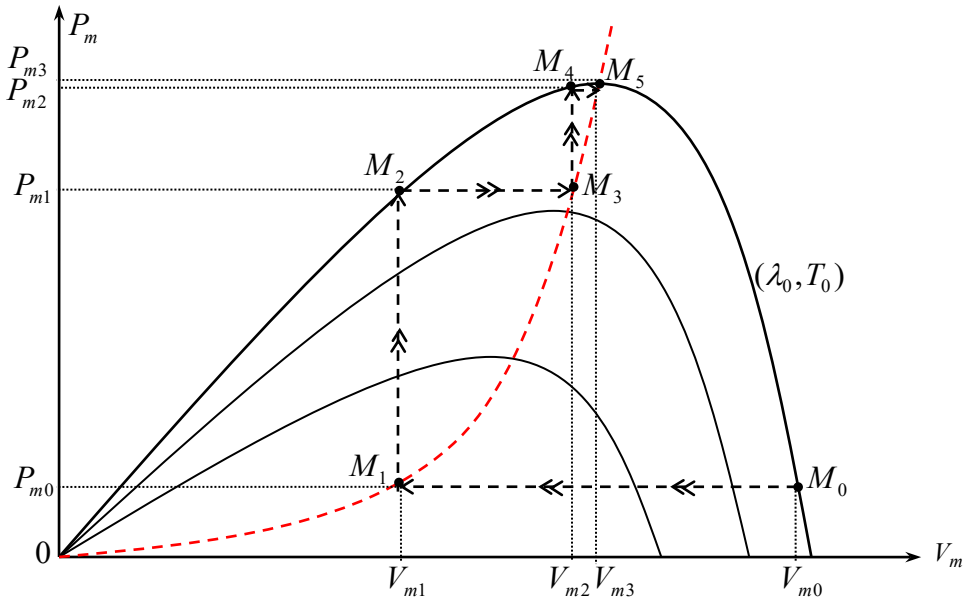

Fig.6: MPP achievement procedure

For convenience, the main result of this paper is summarized in the following theorem.

Theorem 1 (*main result*). Consider the single-phase grid-connected PV system shown in Fig. 2, represented by its average model (3a-d), together with the controller consisting of the control laws (16), (21) and (24a-c), where the voltage V_m is generated by the PV power optimizer (26). Then, one has the following results:

1) The closed loop system is described, in terms of the error variables (z_1, z_2, z_3), by equations (10), (15) and (22), which are rewritten for convenience:

$$\dot{z}_1 = -c_1 z_1 - z_2 \tag{27a}$$

$$\dot{z}_2 = -c_2 z_2 + z_1 \tag{27b}$$

$$\dot{z}_3 = -c_3 z_3 \tag{27c}$$

This system is globally exponentially stable.

2) It readily follows from Part 1 that, the tracking error $z_1 = x_1 - V_m$ vanishes exponentially, implying the achievement of the MPPT requirement.

3) The tracking error $\varepsilon_{dc} = x_3 - V_d$ converges to zero guaranteeing a tight regulation of the dc bus voltage.

4) Also, Part 1 implies the convergence of the error $z_3 = x_4 - x_4^*$ to zero, with $x_4^* = \beta e_g$. On the other hand, the real variable (24a) β converges to a constant. That is, the objective of unity PF is asymptotically ensured.

Proof. Consider the following Lyapunov function candidate

$$V = V_1 + V_2 + V_3 = 0.5z_1^2 + 0.5z_2^2 + 0.5z_3^2 \tag{28a}$$

Using (27a-c), it follows that the time-derivative of V is given by:

$$\dot{V} = -c_1 z_1^2 - c_2 z_2^2 - c_3 z_3^2 \tag{28b}$$

Part 1. From (28a-b) one immediately sees that V is positive definite and $\dot{V}$ is negative definite. Therefore, system (27a-c) with the state vector (z_1, z_2, z_3) is globally asymptotically stable (GAS). Furthermore, as (27a-c) is linear, asymptotic stability is equivalent to exponential stability.

Part 2. This is a direct consequence of Part 1.

Part 3. The PI regulator (24a-b) is resorted to enforce the convergence of the error $\varepsilon_{dc} = x_3 - V_d$ to zero. It follows in turn that β converges to a constant (presence of integral action).

Part 4. The convergence of z_3 to zero is an immediate consequence of Part 1. The convergence of z_3 to zero and the convergence of β to a constant clearly show that the PF is asymptotically ensured.

4. Simulation results

The theoretical performances of the proposed nonlinear controller, already established in Theorem 1, will now be illustrated by simulation. To this end, the experimental setup of Fig. 7 is simulated using MATLAB/Simulink environment. The characteristics of the controlled system are listed in Table 3. Let us emphasize that the controlled system is simulated using the instantaneous model ((1), (2)). The averaged model (3a-d) is in effect used only in controller design. The control design parameters values are given of Table 4 which proved to be convenient.

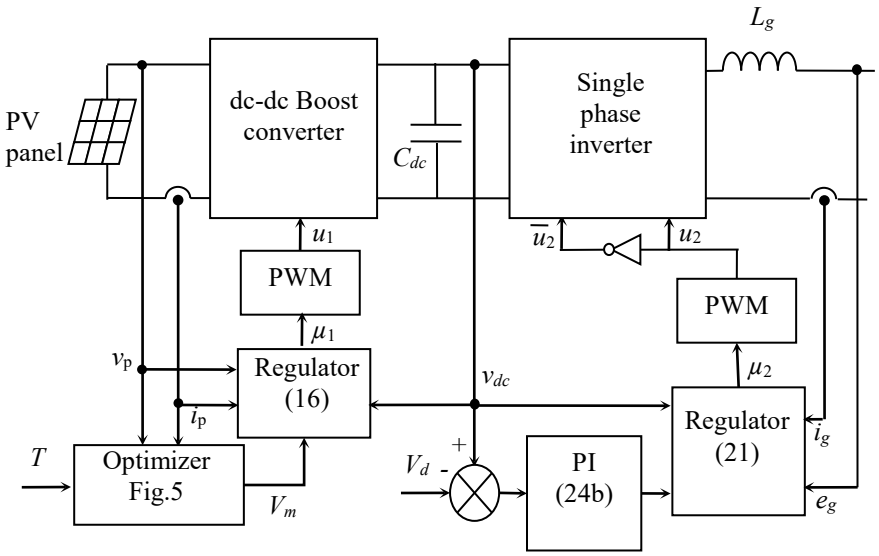

Fig.7: Simulated experimental setup for single phase grid connected system control

Table 3. Characteristics of Controlled System

Parameter	Symbol	Value
PV array	PV model	NU-183E1
	PV power	183.1W
Boost converter	C_i	4700μF
	L_i	1mH
	R_i	0.65Ω
DC link capacitor	C_{dc}	6800μF
Grid filter inductor	L_g	2.2mH
	R_g	0.47 Ω
PWM Switching frequency	f_s	25kHz
Grid	Transformer ratio	22:220
	AC source	220V

Table 4. Controller Parameters

Parameter	Symbol	Value
Design parameters of control laws (16) and (21)	c_1	10^5
	c_2	10^4
	c_3	10^4
PI regulator (G_{pi}) (24b)	k_i	0.02
	τ_i	30ms
Desired DC bus voltage	V_d	48V

The maximum power points (MPP) under climatic conditions (temperature and radiation), for the considered PV array module of type NU-183E1, are shown in Table 5 and will be used in the forthcoming simulation tests.

Table 5. Maximum Power Points (MPP)

MPP	V_m	P_m
M1(λ=1000W/m^2; T=25°C)	23.82 V	183.1 W
M2(λ=600W/m^2; T=25°C)	23.37 V	108.41 W
M3(λ=400W/m^2; T=25°C)	22.94 V	70.8 W
M4(λ=1000W/m^2; T=60°C)	20.38 V	153.4 W
M5(λ=1000W/m^2; T=10°C)	25.17 V	196 W

The resulting closed-loop control performances are illustrated by Fig 8 to Fig 16.

4.1. Radiation change effect

Fig. 8 illustrates the perfect achievement of MPPT in presence of radiation changes. Specifically, the radiation varies between $400\ \mathrm{W/m^2}$ and $1000\ \mathrm{W/m^2}$ at time $0.4s$ and returns to $600\ \mathrm{W/m^2}$ at time $0.8s$, meanwhile the temperature is kept constant, equal to 25°C. The figure shows that the captured PV power varies between $70.8\ \mathrm{W}$ and $183.1\ \mathrm{W}$ at time $0.4s$ and then returns to 108.4 W at time $0.8s$. These values respectively correspond to the maximum points M3, M1 and M2 (see Table 5), on the curves associated to the considered radiations. It is worth noting that the MPPT is achieved very fast comparing to the classical algorithms (Perturb and observe for example). The figure, also shows that the DC bus voltage v_{dc} is regulated to its desired value V_d=48V. Fig. 9 illustrates the grid current i_{Lg} and the grid voltage e_g. A detailed view on the controller behavior around the radiation change (at time 0.4s) is provided by the zoom in Fig. 10. This figure clearly shows that the current i_{Lg} is sinusoidal and in phase with the voltage e_g, proving unity PF achievement.

4.2. Temperature variation effect

Fig. 11 illustrates the controller behavior when facing temperature changes. Specifically, the temperature T varies between 25°C and 60°C at time $0.4s$ and then returns to 10°C, while the radiation λ remains constant equal to $1000\ \mathrm{W/m^2}$. It is seen that the controller keeps the whole system at the optimal operation conditions. Indeed, the captured PV power P achieves, respectively, the values 183.1W, 153.4W and 196W corresponding (see Table 5) to the maximum points (M1, M4 and M5) associated to the considered temperatures, respectively. Also, it is seen that the MPPT is rapidly achieved. The figure also shows that the DC bus voltage v_{dc} is regulated to its desired value V_d=48V. Fig. 12 illustrates the grid current i_{Lg} and the grid voltage e_g. A detailed view on the controller behavior around the temperature change (at time 0.8s) is provided by the zoom of Fig. 13. This figure also shows that the current i_{Lg} is

sinusoidal and in phase with the voltage e_g, which proves the achievement of unity PF.

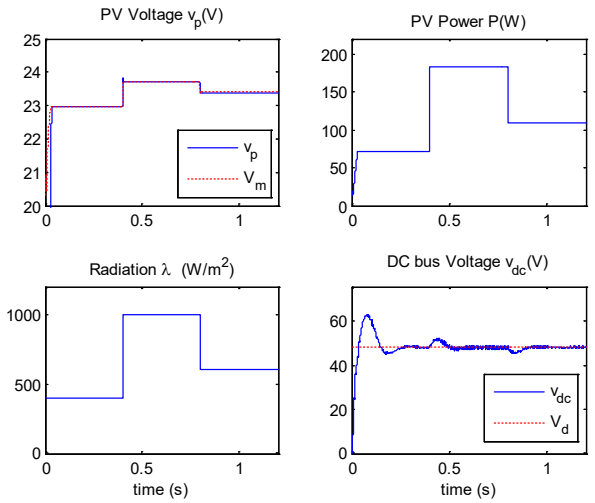

Fig.8 : MPPT and DC bus voltage achievement in presence of radiation changes.

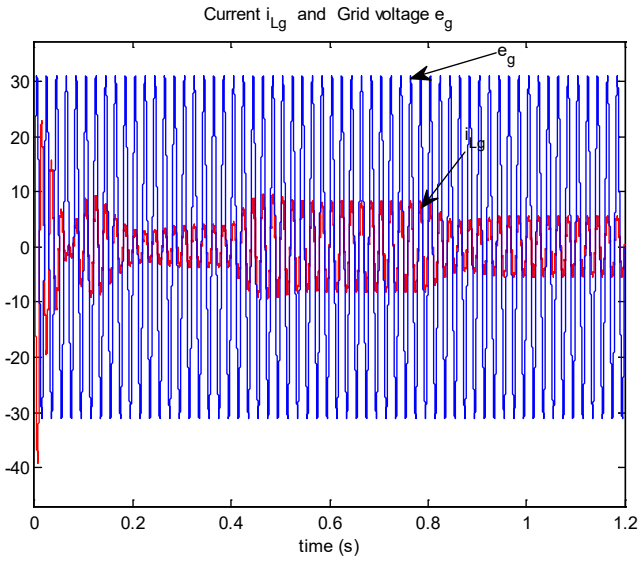

Fig.9. Grid current and voltage in presence of radiation changes

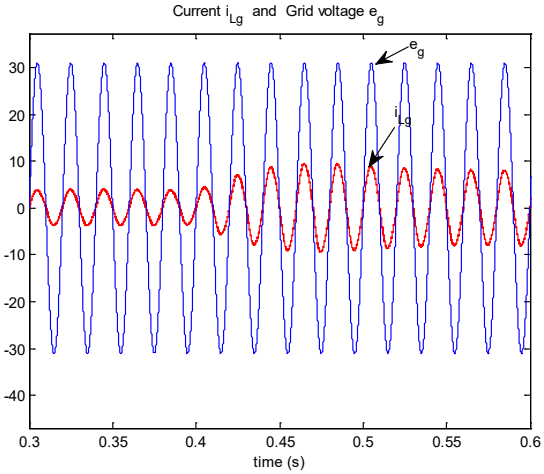

Fig.10. Zoom on the signals of Fig. 9, showing unity PF in presence of radiation changes

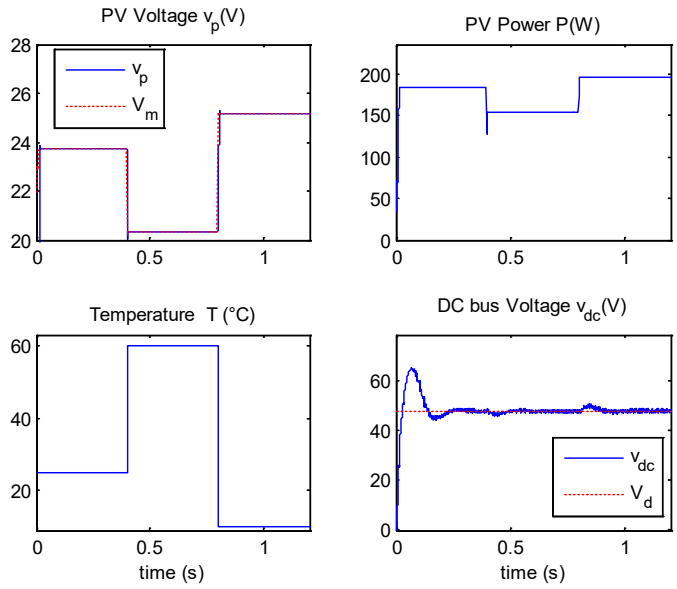

Fig.11. MPPT and DC bus voltage achievement in presence of temperature changes.

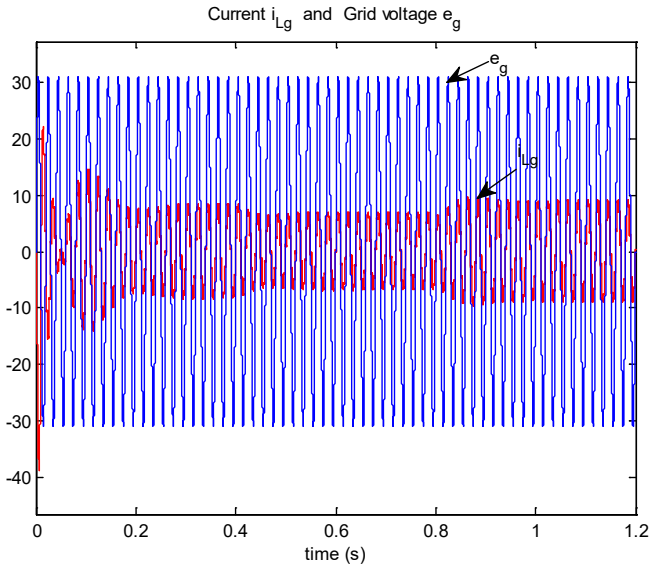

Fig.12 : Grid signals in presence of temperature changes

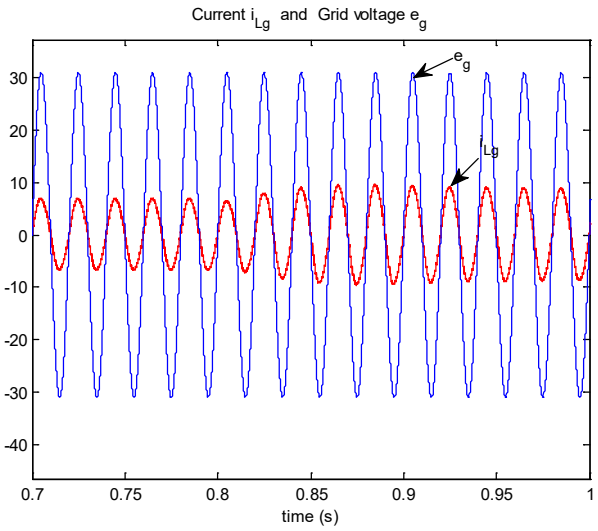

Fig.13. Zoom on the signals of Fig. 12 confirming the achivement of unity PF in presence of temperature changes

4.3. Controller sensitivity to variations of power converter components

The components of power converters may vary even during normal operation conditions, due to changes of operation set points, temperature, etc. Therefore, it is of interest to evaluate the performances of the proposed controller in presence of this uncertainty. Fig.14 illustrates the closed-loop behavior in presence of the variations of the components C_i, L_i, C_{dc} and L_g. Specifically, a 20% change is produced on the true values of these parameters, with respect to their nominal values. Meanwhile, the temperature T and the radiation λ are set to the constant values 25°C and 1000 W/m^2. Note that the change in the component values is only produced on the model simulating the controlled system. The controller design is not concerned by this change i.e. it keeps on using the nominal values. The variations of the parameters C_i, L_i, C_{dc} and L_g are performed at times $0.2s$, $0.4s$, $0.6s$ and $1s$, respectively. The resulting control performances are illustrated by Fig. 14 which shows that the captured PV power keeps on tracking its optimal point, despite the uncertainty on the system component characteristics. This figure also shows that the DC bus voltage v_{dc} is regulated to its desired value $V_d = 48V$ and the current i_{Lg} remains sinusoidal and in phase with the voltage e_g, proving that unity PF is still achieved. These results confirm the controller robustness to system parameter uncertainty.

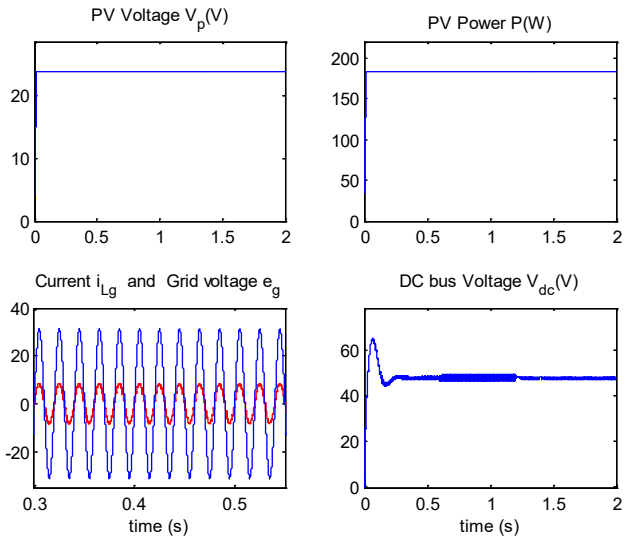

Fig. 14. Illustration of controller robustness against system parameter uncertainties

4.4. Proposed PV power optimizer vs traditional methods

In this section, the supremacy of the proposed PV power optimizer over traditional techniques will now be illustrated. Two traditional techniques are considered i.e. perturb and observe (P&O) and incremental conductance algorithms.

4.4.1. Proposed PV power optimizer vs P&O algorithm

The comparison between the proposed MPPT optimizer and the P&O algorithm [12] is illustrated by Fig.15. The involved parameters in the P&O algorithm are the following: delay $T_d = 10^{-3}$ and control law step $\Delta U = 0.03$. The figure clearly shows that the proposed PV power optimizer is much better, from the rapidity and accuracy viewpoints, than the P&O method.

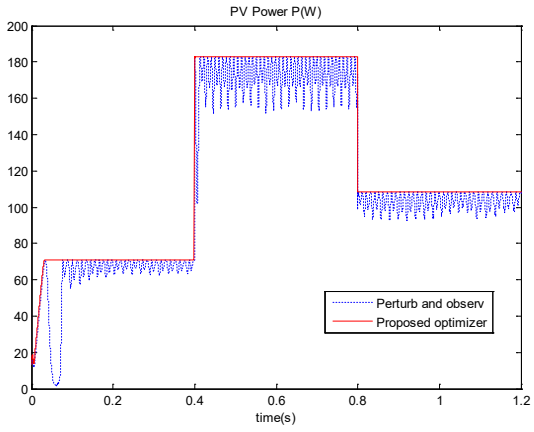

Fig.15: Comparison between the proposed MPPT optimizer and the classic P&O algorithm.

4.4.2. Proposed PV power optimizer vs Incremental Conductance algorithm

Fig. 16 illustrates the MPPT achievement of the proposed strategy and Incremental Conductance algorithm [14,15] in presence of radiation changes. Specifically, the radiation varies between

$400\ \mathrm{W/m^2}$ and $1000\ \mathrm{W/m^2}$ at time $0.4s$ and returns to $600\ \mathrm{W/m^2}$ at time $0.8s$ .The figure clearly shows that the proposed PV power optimizer is much better, from the rapidity and accuracy viewpoints, than the Incremental Conductance method.

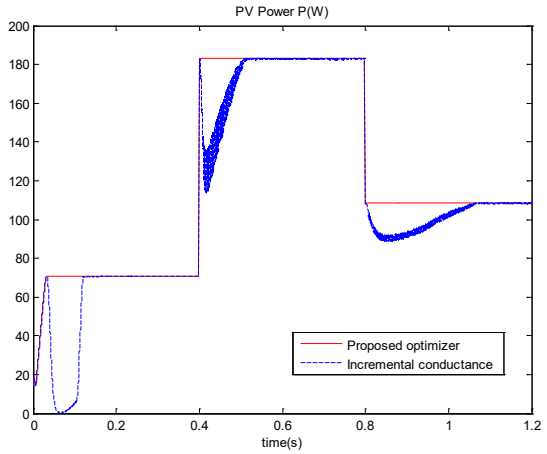

Fig.16: Comparison between the proposed MPPT optimizer and the classic Incremental Conductance algorithm.

5. Conclusion

The problem of controlling a single-phase grid-connected PV system is addressed and dealt with using nonlinear control techniques, on the basis of the nonlinear average model (3). The MPPT problem is coped with by designing a PV power optimizer proving online the controller with the PV optimal voltage. Using both a theoretical analysis and simulation, it is proved that the controller does meet the performances for which it was designed, namely: (i) global asymptotic stability of the closed-loop system, (ii) perfect maximum power point tracking of PV array; (iii) good unity power factor in the grid; (iv) tight regulation of the DC bus voltage.

REFERENCES

1. Krithiga S., N.G. Ammasai Gounden, “Power electronic configuration for the operation of PV system in combined grid-connected and stand-alone modes,” *IET Power Electron.*, Vol. 7, No. 3, pp. 640-647 (2014).
2. Akorede M.F., H. Hizam, E. Pouresmail, “Distributed energy resources and benefits to environment,” *Renew. Sust. Energ. Rev.*, Vol. 14, pp. 724-734 (2010).
3. El Fadil, H. , F. Giri, A. Yahya and H. Erguig, “Nonlinear Control of Hybrid Photovoltaic/Fuel Cell Distributed Generation System,” *Proc. 11th IFAC Int. Workshop Adapt. Learn. Control Signal Process.*, Caen, France, pp. 665-670 (2013).
4. Vahidinasab, V., “Optimal distributed energy resources planning in a competitive electricity market: Multiobjective optimization and probabilistic design,” *Renew. Energ.*, Vol. 66, pp. 354-363 (2014)
5. Guggilam, S. S., C. Zhao, E. Dall’Anese, Y. Christine and S. V. Dhople, “Optimizing Power-frequency Droop Characteristics of Distributed Energy Resources,” *IEEE Trans. Power Syst.*, Vol. PP, No. 99, pp. 1-1 (2017).
6. Mastromauro, R.A., Liserre, M. Kerekes, T. Dell'Aquila, “A Single-Phase Voltage-Controlled Grid-Connected Photovoltaic System With Power Quality Conditioner Functionality,” *IEEE Trans. Indust. Electron.*, Vol. 56, No.11, pp. 4436–4444 (2009).
7. Gu, B., J. Dominic, J.S. Lai, C.L. Chen, T. LaBella, B. Chen, “High reliability and efficiency single-phase transformerless inverter for grid-connected photovoltaic systems,” *IEEE Trans. Power Electron.*, Vol. 28, No. 5, pp.2235-2245 (2013).

8. Yang, Y., F. Blaabjerg, Z. Zou, "Benchmarking of Grid Fault Modes in Single-Phase Grid-Connected Photovoltaic Systems," *IEEE Trans. Ind. Applicat.,* Vol. 49, No. 5, pp.2167-2176 (2013).

9. Hu, H., S. Harb, N.H. Kutkut, Z.J. Shen, I. Batarseh, "A Single-stage microinverter without using eletrolytic capacitors," *IEEE Trans. Power Electron.*, Vol. 28, No (6), pp.2677-2687 (2013).

10. Mahmud, M.A., H.R. Pota, M.J. Hossain, "Nonlinear Current Control Scheme for a Single-Phase Grid-Connected Photovoltaic System," *IEEE Trans. Sust. Energ.,* Vol.5, no.1, pp.218-227 (2014).

11. Li, Y*., and* M. Ishikawa, "Statistical Analysis of Power System Sensitivity Under Random Penetration of Photovoltaic Generation," *Asian J. Control,* Vol. 19, pp. 1688–1698 (2017).

12. Sera D., L. Mathe, T. Kerekes, S.V. Spataru, R. Teodorescu, "On the Perturb-and-Observe and Incremental Conductance MPPT Methods for PV Systems," *IEEE Trans. J. Photovoltaics*, Vol. 3, No. 3, pp.1070-1078 (2013).

13. Fermia, N., D. Granozio, G. Petrone, M. Vitelli, "Predictive & adaptive MPPT perturb and observe method," *IEEE Trans. Aerosp. Electron. Syst.*, Vol.43, No. 3, pp.934-950 (2007).

14. Ishaque K., Z. Salam, G. Lauss, "The performance of perturb and observe and incremental conductance maximum power point tracking method under dynamic weather conditions," *Appl. Energ.*, Vol. 119, pp. 228-236 (2014).

15. Chia-Hung Lin, Cong-Hui Huang, Yi-Chun Du, Jian-Liung Chen, "Maximum photovoltaic power tracking for the PV array using the fractional-order incremental conductance method," *Appl. Energ.*, Vol. 88, No. 12, pp. 4840-4847 (2011).

16. Rajesh, R., M. Carolin Mabel, "Efficiency analysis of a multi-fuzzy logic controller for the determination of operating points in a PV system," *Solar Energ.*, Vol. 99, pp. 77-87 (2014).

17. Ammasai, G. N., S.A. Peter, H. Nallandula, S. Krithiga, "Fuzzy logic controller with MPPT using line-commutated inverter for three-phase grid-connected photovoltaic systems," *Renew. Energ.*, vol. 34 (3), pp. 909-915 (2009).

18. Hassaine L., E. O. Lias, J. Quintero, V. Salas, "Overview of power inverter topologies and control structures for grid connected photovoltaic systems," *Renew. Sust. Energ. Rev.*, Vol. 30, pp. 796-807 (2014).

19. Ravi, A., P.S. Manoharan, J. Vijay Anand, "Modeling and simulation of three phase multilevel inverter for grid connected photovoltaic systems," *Solar Energ.*, Vol. 85 (11), pp. 2811-2818 (2011).

20. Xiong Y., S. Qian, J. Xu, "Single-Phase Grid-Connected Photovoltaic System Based on Boost Inverter," *2012 Asia-Pacific Power. Energ. Eng. Conf. (APPEEC),* pp.1-3, 27-29 (2012).

21. Luo, A., Yandong Chen, Zhikang Shuai, Chunming Tu, "An Improved Reactive Current Detection and Power Control Method for Single-Phase Photovoltaic Grid-Connected DG System," *IEEE Trans. Energ. Conv.*, Vol. 28, No. 4, pp.823-831 (2013).

22. Menti, A., T. Zacharias, J. Milias-Argitis, "Harmonic distortion assessment for a single-phase grid-connected photovoltaic system," *Renew. Energ.*, Vol. 36, No. 1, pp. 360-368 (2011).

23. Wu, L., Z. Zhao, J. Liu., "A single-stage three-phase grid-connected photovoltaic system with modified MPPT method and reactive power compensation," *IEEE Trans. Energ. Conv.*, Vol. 22, No. 4, pp. 881-886 (2007).

24. Enrique, J.M., E. Duran, M. Sidrach-de-Cardona, J.M. Andujar, "Theoretical assessment of the maximum power point tracking efficiency of photovoltaic facilities with different converter topologies," *Solar Energ.*, Vol. 81, pp. 31-38 (2007).

25. Chen-Chi, C., C. Chieh-Li, "Robust maximum power point tracking method for photovoltaic cells: A sliding mode control approach," *Solar Energ.*, Vol.83, pp. 1370–1378 (2009).

26. El Fadil H. and F. Giri, "Climatic sensorless maximum power point tracking in PV generation systems," *Control Eng. Practice*, Vol. 19, No. 5, pp. 513–521 (2011).

27. Oulcaid, M., H. El Fadil, A.Yahya, F. Giri, "Maximum Power Point Tracking Algorithm for Photovoltaic Systems under Partial Shaded Conditions," *Proc. 12th IFAC Int. Workshop Adapt. Learn. Control Signal Process. (ALCOSP-2016)*, Eindhoven, Netherlands, pp. 217-222 (2016).

28. Krein P.T., J. Bentsman, R.M. Bass, B. Lesieutre, "On the use of averaging for analysis of power electronic system," *IEEE Trans. Power Electron.*, Vol. 5, No. 2, pp. 182–190 (1990).

29. Krstic, M., I. Kanellakopoulos and P. V. Kokotović, *Nonlinear and adaptive control design,* John Willy & Sons, NY (1995).

30. Lin, F.-J., S.-G. Chen, I.-F. Sun, "Adaptive Backstepping Control of Six-Phase PMSM Using Functional Link Radial Basis Function Network Uncertainty Observer," *Asian J. Control, doi:* 10.1002/asjc.1521 (2017).

31. Tahri, A., H. El Fadil, F. Giri, F.-Z. Chaoui, "Nonlinear Adaptive Control of a Hybrid Fuel Cell Power System for Electric Vehicles – a Lyapunov Stability Based Approach," *Asian J. Control,* Vol.18, pp. 166–177 (2016).